Investigation on Homogeneous Modeling of Gyroid Lattice Structures: Numerical Study in Static and Dynamic Conditions

Edoardo Mancini[1,a*], Mattia Utzeri[2,b] and Marco Sasso[2,c]

[1]Università degli Studi dell'Aquila, DIIIE, Piazzale Ernesto Pontieri I, Monteluco di Roio, 67100 L'Aquila, Italy

[2]Università Politecnica delle Marche, DIISM, Via Brecce Bianche, 60121 Ancona, Italy

[a]edoardo.mancini@univaq.it; [b]m.utzery@pm.univpm.it; [c]m.sasso@staff.univpm.it;

Keywords: Additive Manufacturing, homogeneous material, lattice structure, Gyroid

Abstract. The TPMS (triply periodic minimal surface) are receiving great attention for production of open cell scaffold structures, for example in biomedical applications. In this paper stretch-dominated lattice structures have been considered. The Gyroid cell made of epoxy resin by DLP technology was analyzed. The compression test results in quasi-static (10^{-3} s^{-1}) and dynamic (4×10^2 s^{-1}) conditions have been used to compute the macroscopic cellular material properties by the homogenization methods. Finally, in order to evaluate the behaviour of the unit cell under multi-axial stress state, combined shear-compression tests have been carried out as well.

Introduction

The gyroid, one of triply periodic minimal surface (TPMS), belongs to the cubic crystal system, which was described in [1] and designed for lightweight high-strength new materials. Gyroid structures can be sheet-based and strut-based [2]. In this work, sheet-based gyroid cellular structures are designed and manufactured by Digital Light Processing (DLP).

The mechanical response of lattice scaffold structures can be numerically evaluated either studying the unit cell [3][4] or implementing a homogeneous material model able to reproduce the lattice mechanical behaviour. As a matter of fact, the structural behaviour of components built of lattice unit cells and, in general, of cellular materials is very hard to be analysed numerically, due to the necessity to reproduce the real structure. The adoption of mesoscopic modelling usually determines a computational cost not negligible [5][6], so, the capability to use a homogeneous material model able to reproduce lattice behaviour may overcome this limitation. Homogenization method can be used to compute the macroscopic cellular material properties so to replace mesoscopic ones. Moreover, the anisotropy of the structures must be evaluated when cellular materials are used.

In this paper the numerical homogenization following the periodical RVE proposed by Xia et al [7] and Kadri et al [8], was used. The unit cell C8 (8x8x8 mm) was taken as representative volume element (RVE) and then modelled to calculate the elastic tensor for the homogeneous formulation. The same cell was adopted for the mesoscopic numerical models.

After the numerical mesoscale model validation, different simulations have been carried out to access the gyroid cell behaviour at a different loading direction. The simulated compression tests of the structures, oriented in a different direction, to reproduce combined shear-compression, have been prepared and analysed.

Material and method

Material. All specimens and scaffolds were printed through a commercial DLP 3D printer Anycubic Photon S (Fig. 1). The material is a commercially available high-quality resin product (Value, Prima Creator) [3].
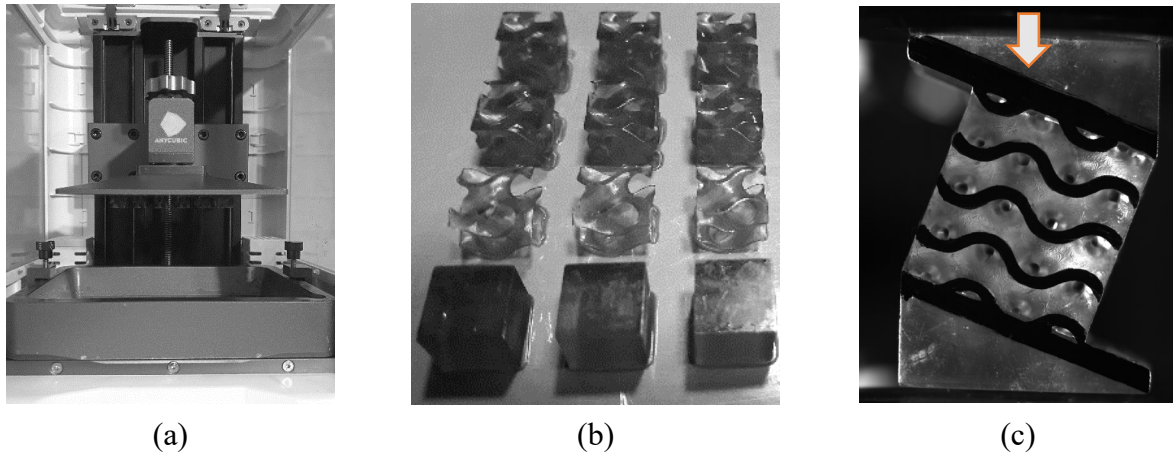
Fig. 1 3D printing: (a) Anycubic 3D printer, (b) Printed specimens (Reproduced from [3], Fig. 1) and (c) scaffolds for combined shear-compression

The features of the cells and scaffolds are reported in Table 1. The cellular structures were of TPMS Gyroid type, with different sizing but similar density. The Gyroid structures were designed into Ntopology™ software. Then, the STL format files of all structures were exported to the FE model software Hypermesh.

Table 1 Gyroid samples

	Dimension [mm]	Cell	Thicknesses [mm]	Designation
Unit cell 8	8x8x8	8	1	C8
Scaffold unit cells 8	16x16x16	8	1	S16C8

The unit cell and the scaffolds, the latter for combined shear-compression tests, has been printed with the same parameters as in [3] (cf. Table 1).

Equipment. Quasi-static compression and combined shear-compression tests were performed by a universal tensile machine equipped with a 50kN load cell (Zwick/Roell® Z050, Fig. 3a). Dynamic compression test have been carried out by a direct split Hopkinson bar (Fig. 3b) available at the lab of Polytechnic University of Marche [9][10].
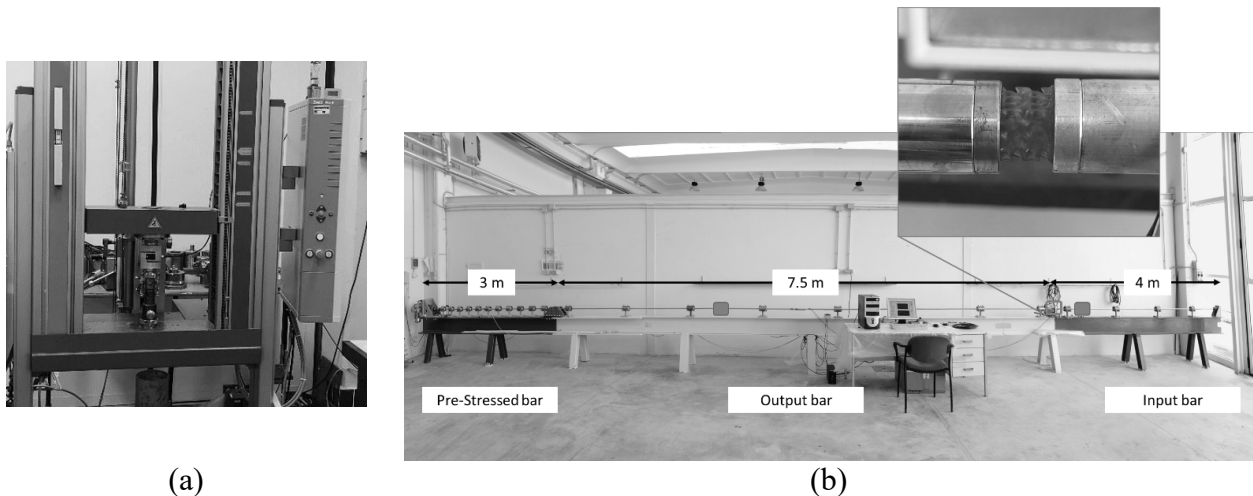

Fig. 2 Equipment (a) Tensile machine, (b) Hopkinson bar (Reproduced from [3], Fig. 3)

Finite Element Model. 3D mesoscale and macroscale FE model have been carried out to calculate the stiffness matrix by homogenization procedure, to assess the effects of combined loads and to verified the homogenization procedure itself. The material law has been modeled as piecewise linear

obtained experimentally by the authors in [3] for mesoscopic models, whereas the linear elastic-anisotropic material was used for macroscale simulation.

The *Bi-linear law*, expressed by equation (1), was chosen. The material model coefficients have been parametrized as a function of the relative density ($\rho_{rel} = \rho_{eff}/\rho_{bulk}$; ρ_{eff} is the gyroid density and ρ_{bulk} is the density of base material).

$$\begin{aligned} \sigma &= E(\rho_{rel})\varepsilon & \sigma \leq \sigma_y \\ \sigma &= \sigma_y(\rho_{rel}) + E_T(\rho_{rel})(\varepsilon - \varepsilon_y) & \sigma \geq \sigma_y \end{aligned} \tag{1}$$

where σ and ε are engineering stress and strain considered positive in compression and E, E_T, ε_y and σ_y are the Young Modulus, Tangent Modulus, Strain at Yield and Yield Strength, respectively.

Tetrahedral elements with a mean size of 0.3 mm have been used. All FE models are reported in Fig. 3. The model in Fig. 3b was used to confirm the utility of mesoscale modelling, despite, leaving the computational cost very high. Instead, the model in Fig. 3c has been necessary to limit the scaffold supports effect.
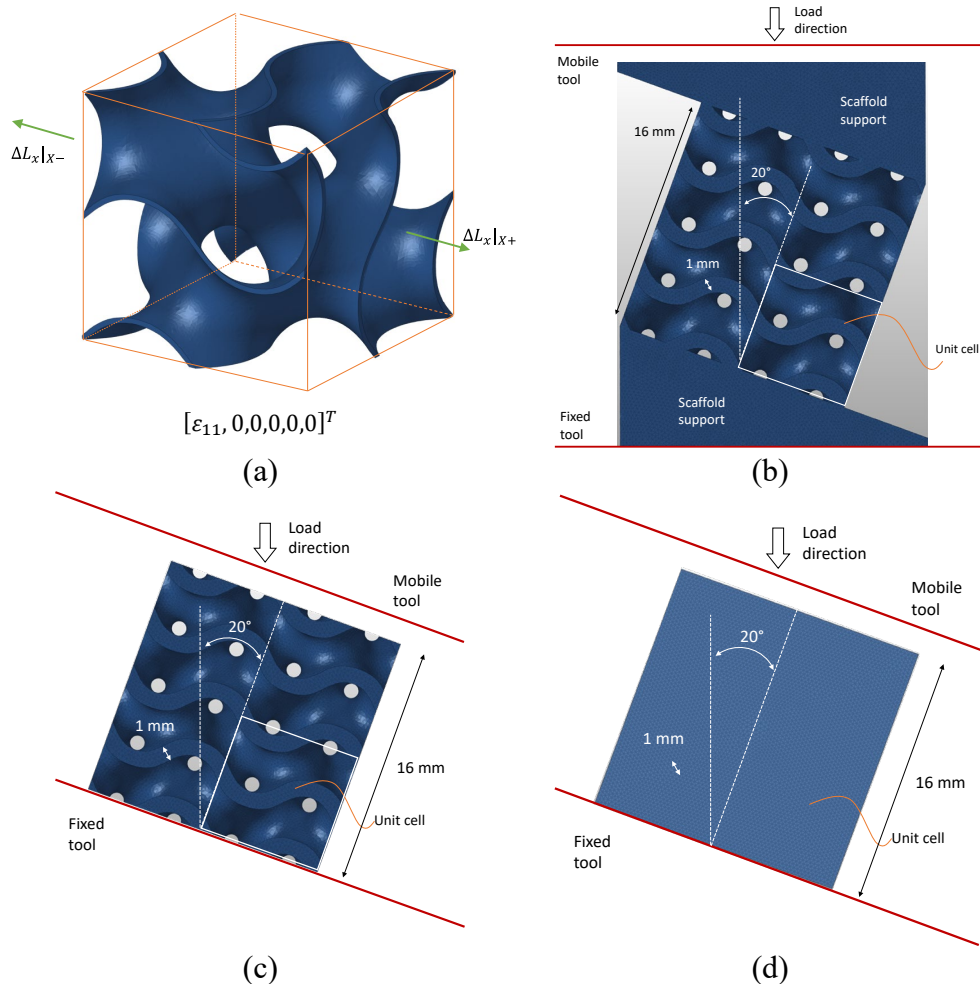

Fig. 3 FE model: (a) unit cell 8 for homogeneous - formulation, (b) mesoscopic model for numerical verification, (c) mesoscopic and (d) macroscopic models for combine shear-compression tests comparison

To calculate the elastic tensor *Cij* (stiffness matrix) for the homogeneous formulation the simple procedure described in [7] and [8] was taken. The unit cell C8 as representative volume element (RVE) was chosen and modelled. The unified periodic boundary condition reported in equation Eq.(2) was adopted.

$$\Delta l^+{}_{x,y,z}|\hat{\imath},\hat{\jmath},\hat{\varkappa} - \Delta l^-{}_{x,y,z}|\hat{\imath},\hat{\jmath},\hat{\varkappa} = D^{(x,y,z)}_{[\hat{\imath},\hat{\jmath},\hat{\varkappa}]} \qquad (2)$$

where $\hat{\imath}, \hat{\jmath}$ and $\hat{\varkappa}$ are the cosines directors of axes x, y and z, $\Delta l^+{}_{x,y,z}|\hat{\imath},\hat{\jmath},\hat{\varkappa}$ is the displacement of nodes on the RVE surfaces whose normal are $\hat{\imath}, \hat{\jmath}$ and $\hat{\varkappa}$, $\Delta l^-{}_{x,y,z}|\hat{\imath},\hat{\jmath},\hat{\varkappa}$ is the displacement of nodes on opposite face of the RVE (Fig. 4). The constants, $D^{(x,y,z)}_{[\hat{\imath},\hat{\jmath},\hat{\varkappa}]}$ represent both the average stretch or contraction of the RVE model due to the action of the three normal traction components and the shear deformations due to the three shear traction components.
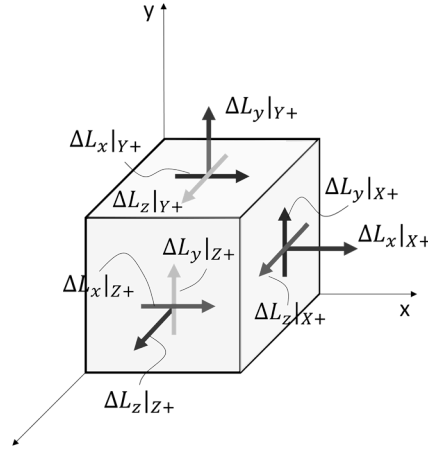

Fig. 4 Displacement notations

The effective elasticity tensor *Cij* was calculated by solving the material constitutive relation Eq.(3) by applying strain loadings on the mesoscopic unit cell model:

$$\sigma_i = C_{ij}\varepsilon_j \quad (i, j = 1 \text{ to } 6) \qquad (3)$$

where σ_i and ε_j are the stress and strain of the RVE model. To solve Eq. (3), the following six loadings were applied individually in the RVE models (e.g. ε_{11} is shown in Fig. 3a).

$$\varepsilon_{11} = [0.02,0,0,0,0,0]^T \quad \varepsilon_{22} = [0,0.02,0,0,0,0]^T \quad \varepsilon_{33} = [0,0,0.02,0,0,0]^T$$
$$\varepsilon_{12} = [0,0,0,0.02,0,0]^T \quad \varepsilon_{23} = [0,0,0,0,0.02,0]^T \quad \varepsilon_{31} = [0,0,0,0,0,0.02]^T$$

σ_i are calculated using the total reaction force divided by the cross-sectional area of the cell (Fig. 5).
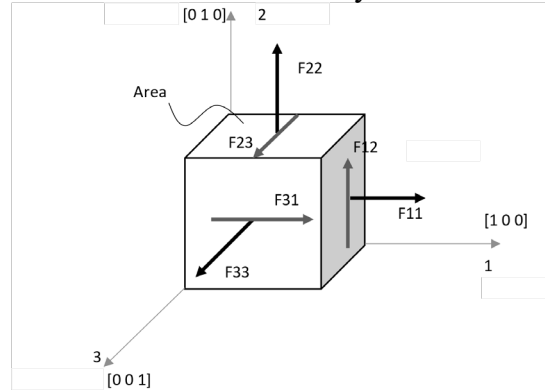

Fig. 5 Reaction forces

Results and Discussion

Quasi-Static and Dynamic behaviour. For what concern the behaviour of the base material in bulk form we used the results, showed in Fig. 6, obtained in a previous work [3].
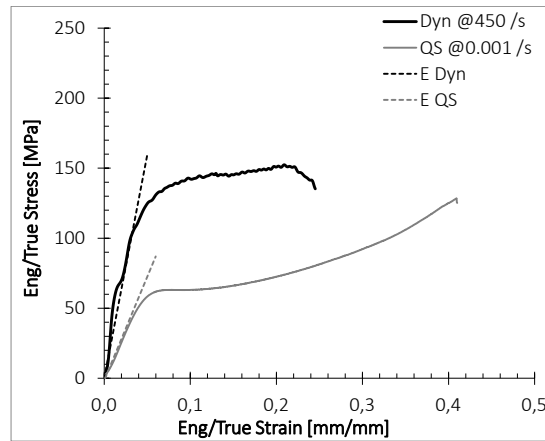
Fig. 6 True. Stress-Strain curves of the base material (Reproduced from [3], Fig. 8; where Dyn @450/s and E Dyn means the reached strain rate and the Young modulus in dynamic conditions, instead QS @0.001 /s and E QS refer to quasi-static conditions)

The scaffold was tested only in quasi-static conditions and to verify the accuracy of the numerical simulation (Fig. 7a). The combined shear-compression test was simulated by placing the scaffolds between the two supports, loaded by two rigid planes (Fig. 3b). A frictional contact with $\mu_s = 0.08$ was imposed between the rigid planes and the supports.

The combined shear-compression results both experimental and numerical are reported in term of load-displacement curves in Fig. 7b. The latter points out the good response of the numerical model.
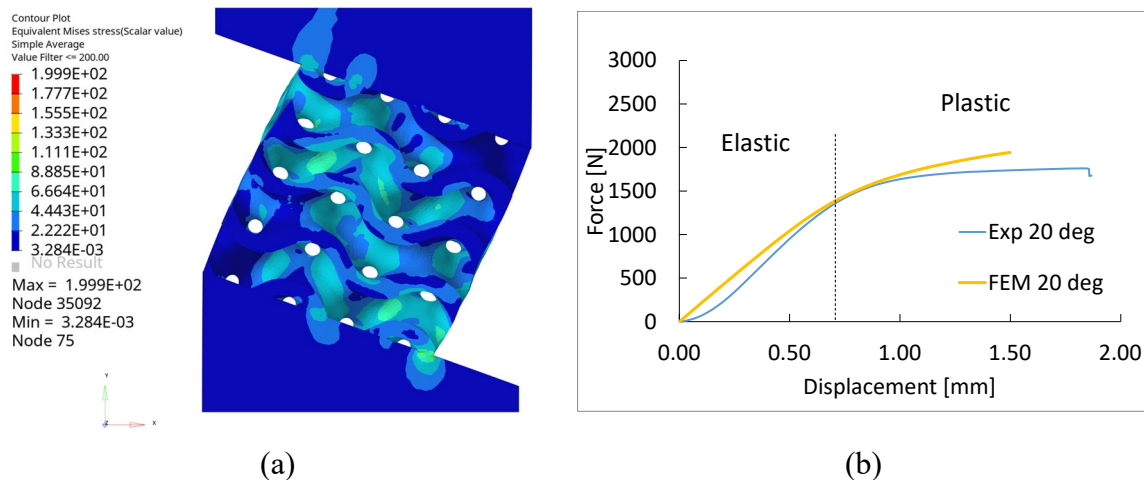

(a)   (b)

Fig. 7 (a) Numerical simulation result (Von Mises stress distribution), (b) Load-displacement curves comparison

Numerical homogenization on unit cell C8. Mesoscopic numerical models have been prepared on unit cell 8 and ρ_{rel} ~0.365 in order to identify the elastic matrix coefficients (Cij). The results confirmed 7 independent constants with C14, C15, C16, and C45 close to zero (Fig. 8 and Fig. 9). Moreover, the Zener factor ($Z = 2C_{44}/(C_{11} - C_{12})$, [11]) was evaluated to identify the anisotropic behaviour. Under quasi-static conditions, the Zener factor was found to be 1.037, which is sufficiently close to unity to consider the Gyroid behaviour as isotropic in the elastic range; on the contrary, anisotropic behaviour is found in dynamic conditions, where the Zener factor has been estimated to be approximately 1.24.

Cij	255.2	100.0	100.0	0.4	5.1	0.3
		255.2	100.0	0.3	0.4	5.1
			255.3	5.1	0.3	0.4
				80.5	0.5	0.5
					80.5	0.5
						80.6

Fig. 8. Gyroid elastic stiffness (Cij) for quasi-static behaviour

Cij	530.8	228.1	225.3	0.6	12.5	0.8
		530.8	228.1	0.8	0.7	12.4
			531.1	12.6	0.9	0.6
				187.5	1.2	1.2
					187.3	1.4
						187.4

Fig. 9 Gyroid elastic stiffness (Cij) for dynamic behaviour

Simulation results. Both mesoscale and macroscale of scaffold S16C8 have been considered. For macroscale simulations two different material models were adopted: the first one was the linear elastic-isotropic material, defined in [3] as function of ρ_{rel} ($E = m_E \cdot \rho_{rel} + q_E$; where m_E, q_E are reported in Table 4 in [3]) whereas, the second one was the linear elastic-anisotropic material model (*Cij*). The relative density ρ_{rel} ~0.365 to represent the S16C8 structures has been studied. The use of the bi-linear material for the elastic part is justified from the Zener factor close to unity. To reduce the computational cost and limit their effects the scaffold supports have been removed and only the sample was considered (Fig. 3c and Fig. 3d).

The results in terms of von Mises equivalent stress are reported in Fig. 10. The absence of results about the macroscale simulation in dynamic condition is related to the material model calibration that is currently under investigation.
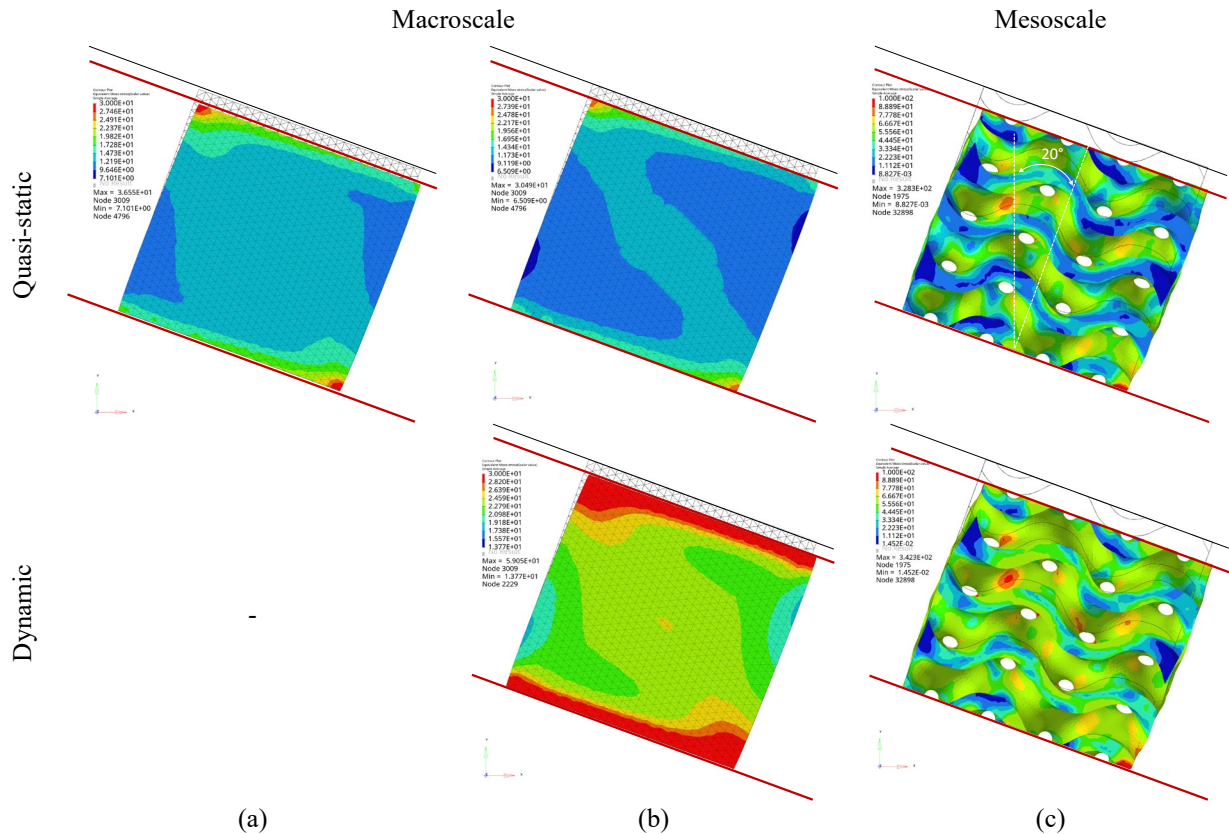
Macroscale   Mesoscale

(a)   (b)   (c)

Fig. 10 Simulation results; (a) Bi-linear material model, (b) Cij stiffness matrix, (c) Base material

Fig. 11 reports the results of the homogenization and Bi-linear formulation superposed on mesoscale load-displacement curves. The results confirmed the optimum homogenization process and the isotropic behaviour of Gyroid in the elastic range for quasi-static tests. A slight discrepancy, as expected, is present for Gyroid behavior in dynamic condition being the Zener factor far from unity. It must be admitted that the homogenization process is likely to suffer from the known difficulties of identifying the correct Young's modulus in dynamic tests.
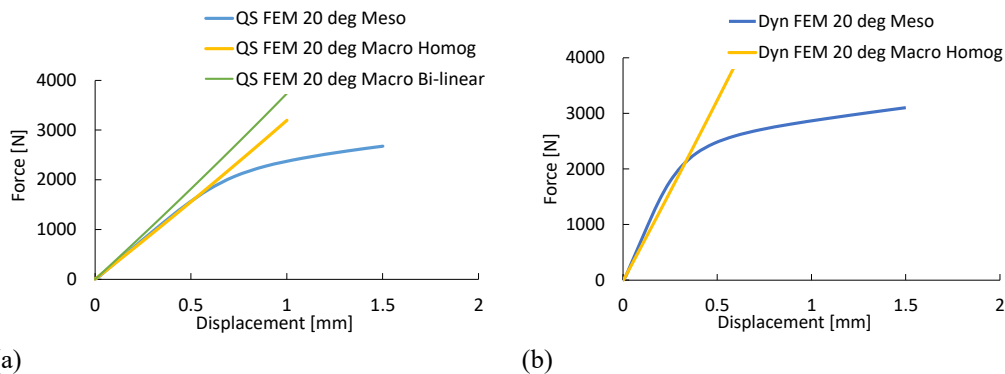

(a)   (b)

Fig. 11 Load-displacement curves: comparison between meso and macro-scale numerical simulations for combined shear-compression loads

Conclusion

In this paper the triply periodic minimal surfaces unit cells, the cubic Gyroid one, was considered. The effect of a load direction different from principal unit cell ones was evaluated too. For the material homogenization the unit cell C8 was chosen as RVE; the quasi-static and dynamic compression tests on base material have been used to identify the elastic modulus.

The results highlighted the capability of the homogeneous formulation to study porous structures made of 3D printed Gyroid surfaces allowing to greatly simplify the FEM modelling process of

complex lattice structures. Moreover, the Zener factor close to unity justifies the use of the bi-linear material model defined in a previous work in quasi-static conditions.

Instead, a small discrepancy is present in dynamic conditions. More attention and further investigations must be carried out for the Young modulus evaluation in dynamic tests.

References

[1] H. Shoen, Alan, Infinite Periodic Minimal Surface without Intersections, NASA. (1970).

[2] D. Li, W. Liao, N. Dai, Y.M. Xie, Absorption of Sheet-Based and Strut-Based Gyroid, Materials (Basel). (2019).

[3] E. Mancini, M. Utzeri, E. Farotti, M. Sasso, Model Calibration of 3D Printed Lattice Structures, ESAFORM 2021. 24th International Conference on Material Forming, Liège, Belgique. 16 (2021) 1–13. doi: 10.25518/esaform21.415416

[4] D.W. Abueidda, M. Bakir, R.K. Abu Al-Rub, J.S. Bergström, N.A. Sobh, I. Jasiuk, Mechanical properties of 3D printed polymeric cellular materials with triply periodic minimal surface architectures, Mater. Des. 122 (2017) 255–267. https://doi.org/10.1016/j.matdes.2017.03.018.

[5] M. Smith, Z. Guan, W.J. Cantwell, Finite element modelling of the compressive response of lattice structures manufactured using the selective laser melting technique, Int. J. Mech. Sci. 67 (2013) 28–41. https://doi.org/10.1016/j.ijmecsci.2012.12.004.

[6] G. Dong, Y. Tang, Y.F. Zhao, A 149 Line Homogenization Code for Three-Dimensional Cellular Materials Written in MATLAB, J. Eng. Mater. Technol. Trans. ASME. 141 (2019). https://doi.org/10.1115/1.4040555.

[7] Z. Xia, Y. Zhang, F. Ellyin, A unified periodical boundary conditions for representative volume elements of composites and applications, Int. J. Solids Struct. 40 (2003) 1907–1921. https://doi.org/10.1016/S0020-7683(03)00024-6.

[8] O.E. Kadri, C. Williams, V. Sikavitsas, R.S. Voronov, Numerical accuracy comparison of two boundary conditions commonly used to approximate shear stress distributions in tissue engineering scaffolds cultured under flow perfusion, Int. j. Numer. Method. Biomed. Eng. 34 (2018) 1–15. https://doi.org/10.1002/cnm.3132.

[9] H. Kolsky, An Investigation of the Mechanical Properties of Materials at very High Rates of Loading, Proc. Phys. Soc. Sect. B. 62 (1949) 676–700. https://doi.org/https://doi.org/10.1088/0370-1301/62/11/302.

[10] E. Mancini, M. Sasso, M. Rossi, G. Chiappini, G. Newaz, D. Amodio, Design of an Innovative System for Wave Generation in Direct Tension–Compression Split Hopkinson Bar, J. Dyn. Behav. Mater. 1 (2015) 201–213. https://doi.org/10.1007/s40870-015-0019-1.

[11] C.M. Zener, S. Siegel, Elasticity and Anelasticity of Metals, J. Phys. Colloid Chem. 53 (1949) 1468–1468. https://doi.org/10.1021/j150474a017.